Synthetic dimensions in optical cavities and their analogies to two-dimensional materials

Giuseppe Pirruccio [1] and Gerardo G. Naumis [2]
[1]*Departamento de Física-Química, Instituto de Física, Universidad Nacional Autónoma de México (UNAM), Apdo. Postal 20-364, 01000 México, CDMX, México*
[2]*Departamento de Sistemas Complejos, Instituto de Física, Universidad Nacional Autónoma de México (UNAM), Apdo. Postal 20-364, 01000 México, CDMX, México*

(Received 31 March 2022; revised 17 June 2022; accepted 18 July 2022; published 29 July 2022)

A method to produce synthetic dimensions in an optical cavity is presented. The system is obtained by coupling two one-dimensional optical cavities by means of a moving mirror. Its translation generates a new synthetic dimension resulting in a transmittance pattern that corresponds to the energy dispersion of electrons in a two-dimensional lattice: in this case a strained triangular lattice. We elucidate the analogy between these two systems by relating the distribution of transmittances of the optical cavity to the density of states of the two-dimensional lattice and the Bragg diffraction modes to the Van Hove singularities. Our mapping makes the coupled optical cavity a simulator for lattice Hamiltonians found in solid-state physics, providing an easier alternative platform to access some of their properties, as for example, the electronic conductivity, which is found here using the Boltzmann formula. Moreover, it is proved that the truly synthetic behavior appears only when the two cavities have an irrational length ratio as modes resonant on one cavity are never resonant in the other. Mathematically, wave phase differences act independently as they are given by a function that behaves as a pseudorandom number generator. This provides an elegant way to study synthetic dimensions without the need to move the central mirror, i.e., in a single, fixed geometry device. Thus, our work establishes a bridge between the fields of optical cavities, synthetic dimensions, and two-dimensional materials.

DOI: 10.1103/PhysRevB.106.035155

I. INTRODUCTION

Although a physical system is commonly described in terms of its geometric dimensionality, during recent years there has been a growing interest in exploring systems exhibiting physics exclusively found in a space with a higher dimensionality than the geometrical one [1–3]. Such concept is known as synthetic dimension [3,4]. Quasicrystals are good examples of an atomic system with synthetic dimensions as their reciprocal space has a higher dimensionality than the real one [5–7]. Other examples are the generation of extra dimensions using magnetic fields or rotated two-dimensional (2D) layers [8]. Yet, in these atomic systems it is difficult to track down the effects of a higher dimension and it has also been difficult to take advantage of them to build devices.

Conversely, in the field of photonics, such effort has been very fruitful [3,9]. For example, photonics allows one to explore the four-dimensional quantum Hall effect [10], flat-band physics [11], topological insulators [12], topological lasers [13], the control of the light spectrum in synthetic space [14,15], and locally interacting [16] and squared effective Hamiltonians [17]. Effects predicted to occur in quasicrystals are also easier to observe [18,19]. A different path to obtain synthetic dimensions and reveal topological invariants is to exploit the time-driven physics of two-dimensional (2D) systems [20–22]. Other ways to dynamically introduce synthetic dimensions in optical systems rely on the use of additional frequencies: electro-optic modulators or spatial light modulators are used to couple longitudinal modes in ring cavities and modes with orbital angular momentum, respectively [23,24].

Such intriguing physics has been often proposed and demonstrated in complex structures either composed by elaborated elementary building blocks or interconnected in a highly nontrivial way. Despite their simplicity, planar 2D cavities exhibit great potential because they enhance light-matter interaction in relatively small volumes and are easy to fabricate. For these reasons, they are often referred to as the paradigmatic cavity in quantum electrodynamics. Recently, they have been used in combination with active media such as inorganic materials [25], quantum wells [26], 2D materials [27], and organic molecules [28], to realize analogies of phenomena encountered in the ultracold atoms literature and believed to be exquisitely quantum. Examples of this are quantum phase transitions of polaritons [29], superfluidity [30], quantum turbulence [31], and in general the realization of quantum simulators [32]. Planar cavities have been also useful to achieve low-threshold lasing emission [33] and enhancing otherwise weak nonlinear interactions between molecules [34,35]. In other interesting applications, planar cavities have been exploited to boost the rate of certain photoactivated reactions giving rise to the so-called polariton chemistry [36,37]. All these applications rely on the remarkable ability of 2D cavities to efficiently confine light on submicron scales by means of the excitation of cavity modes with large quality factors and different symmetry of the

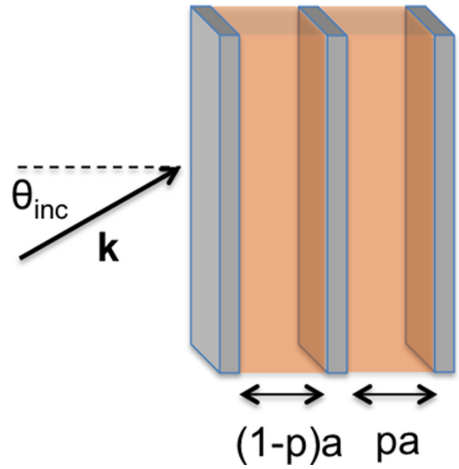

FIG. 1. Sketch of the coupled optical cavities. The thin slabs represent three silver mirrors. a is the sum of the two cavity lengths which are given in terms of p ($0 < p \leqslant 1$). Light of wave vector $\boldsymbol{k}$ illuminates the cavity forming an angle of incidence θ_{inc} with respect to the normal to the multilayer system.

associated electric field. Furthermore, it is simple to build a network of several such cavities by leveraging their planar geometry, which naturally allows for vertical stacking and careful positioning of intermediate mirrors that function as coupling elements.

In this work, we explore the use of geometry to introduce a synthetic dimension in an optical system. This is composed of two planar optical cavities of different lengths separated by a mirror. The translation of the mirror couples the optical modes of the individual cavities generating an extra dimension. We show how it is possible to find the distribution of transmittance, a higher dimensional Bragg law, and some analogies to the energy dispersion of a 2D electronic system, thus drawing an analogy between the fields of 2D materials and optical cavities. As we will see, the truly synthetic dimension behavior appears only for irrational ratios of the two cavity lengths. The layout of this work is the following. In Sec. II we present the the coupled cavities, find the transmittance of the multilayer, and explore the distribution of transmittances. In Sec. III we present the analogy with a 2D system. Section IV is devoted to study irrational length ratios and, finally, the conclusions are given in Sec. V.

II. COUPLED OPTICAL CAVITIES

Figure 1 sketches the proposed cavity. It is made by three parallel silver mirrors and two nonabsorbing dielectrics. In what follows we refer to each space between a pair of contiguous mirrors as left and right cavity. Without loss of generality, we consider both cavities as filled with air. In actual devices this can be replaced by a polymer, for instance. The mirror thickness is fixed and equal to d_1, while the dielectric thickness is defined by the position of the central mirror and parametrized by the variable p bounded between 0 and 1. The total cavity length is a. Light illuminates the double cavity with an angle of incidence θ_{inc} and a wavelength λ. In order to maximize the coupling between the two cavities we fix d_1 to a value at which the normal incidence reflectance of the silver mirrors is 0.5. This corresponds to $d_1 = 13$ nm for $\lambda = 535$ nm. Although this is strictly true only in a range of approximately 15° around the normal incidence, the higher reflectance for larger angles of incidence does not affect our conclusions. The mirrors are described by the experimental permittivity of silver implying an absorption equal to 3% for the incident wavelength. Crucially, we will show that these semitransparent, low-absorbing mirrors effectively generate an extended 2D lattice, whose unit cell consists of the coupled one-dimensional (1D) right and left optical cavities. The incident wavelength, the mirror thickness, and material are chosen to be close to current experimental possibilities.

The transmittance of the two coupled 1D cavities can be obtained with a transfer matrix approach where each medium and interface between them are represented by matrices [38]. We start by describing the left cavity medium (that we label medium 0),

$$P_L = \begin{pmatrix} e^{i\phi_L} & 0 \\ 0 & e^{-i\phi_L} \end{pmatrix} \tag{1}$$

with $\phi_L = k_{\perp,L} d_L$, $d_L = (1-p)a$ and $k_{\perp,L} = n_0 \frac{\omega}{c} \cos\theta_L$ is the perpendicular component of the incident wave vector, $\boldsymbol{k}$, in the left cavity. $\omega = 2\pi c/\lambda$ is the angular frequency of the incident light, c is the speed of light in vacuum, n_0 is the cavity complex refractive index, which in our case equals to 1, and θ_L is the angle of incidence to the left cavity related to θ_{inc} by Snell's law. A similar description holds for the right cavity using the same medium 0,

$$P_R = \begin{pmatrix} e^{i\phi_R} & 0 \\ 0 & e^{-i\phi_R} \end{pmatrix}, \tag{2}$$

where $\phi_R = k_{\perp,R} d_R$, $k_{\perp,R} = n_0 \frac{\omega}{c} \cos\theta_R$ and $d_R = pa$. θ_R is the angle of incidence to the right cavity and is related to θ_{inc} and θ_L by Snell's law.

The mirrors are labeled as medium 1. Inside them the light propagation is described by

$$P_1 = \begin{pmatrix} e^{i\phi_1} & 0 \\ 0 & e^{-i\phi_1} \end{pmatrix}, \tag{3}$$

where $\phi_1 = k_{1,\perp} d_1$, $k_{1,\perp} = (\omega/c) n_1 \cos\theta_1 = \sqrt{(n_1\omega/c)^2 - k_\parallel^2}$, is the perpendicular component of the incident wave vector, $\boldsymbol{k}$. θ_1 is the angle within the mirror, n_1 is the silver complex refractive index, and

$$k_\parallel = \frac{n_0 \omega}{c} \sin\theta_{\text{inc}} \tag{4}$$

is the parallel component of the incident wave vector. Notice that for the parallel component, we do not use a subindex to differentiate the media as this component is conserved. The multilayer system is assumed to be embedded in air, thus the incident medium and the left and right cavities share the refractive index, yielding $\theta_{\text{inc}} = \theta_L = \theta_R = \theta_0$. It follows that

$$k_{\perp,L} = k_{\perp,R} \equiv \kappa,$$

where κ is thus defined as the perpendicular component of $\boldsymbol{k}$ in medium 0. Next, we describe all the interfaces between the media. For s polarization we define two matrices:

$$D_0 = \begin{pmatrix} 1 & 1 \\ n_0\cos\theta_0 & -n_0\cos\theta_0 \end{pmatrix} \tag{5}$$

and

$$D_1 = \begin{pmatrix} 1 & 1 \\ n_1\cos\theta_1 & -n_1\cos\theta_1 \end{pmatrix}. \tag{6}$$

The incidence from medium 1 to 0 is described by

$$T_{10} = D_1^{-1} D_0, \tag{7}$$

while from 0 to 1 the corresponding matrix is

$$T_{01} = D_0^{-1} D_1 = T_{10}^{-1}. \tag{8}$$

In an explicit form, these matrices read as

$$T_{10} = \frac{1}{2}\begin{pmatrix} 1+n_e^{-1} & 1-n_e^{-1} \\ 1-n_e^{-1} & 1+n_e^{-1} \end{pmatrix} \tag{9}$$

and

$$T_{01} = \frac{1}{2}\begin{pmatrix} 1+n_e & 1-n_e \\ 1-n_e & 1+n_e \end{pmatrix} = T_{10}^{-1}, \tag{10}$$

where

$$n_e \equiv \frac{n_1}{n_0}\frac{\cos\theta_1}{\cos\theta_0}.$$

The total transfer matrix along the system is

$$M = [T_{01}P_1T_{10}]P_L[T_{01}P_1T_{10}]P_R[T_{01}P_1T_{10}] \tag{11}$$

or by using Eq. (7),

$$M = \left[T_{10}^{-1}P_1T_{10}\right]P_L\left[T_{10}^{-1}P_1T_{10}\right]P_R\left[T_{10}^{-1}P_1T_{10}\right]. \tag{12}$$

The terms inside brackets represent the complete description of the mirrors and the interface with the cavities. Therefore, we introduce a new matrix such that

$$M = \mathcal{P}P_L\mathcal{P}P_R\mathcal{P} \tag{13}$$

with

$$\mathcal{P} = T_{10}^{-1}P_1T_{10}. \tag{14}$$

The explicit form of such mirror matrix is

$$\mathcal{P} = \frac{1}{4}\begin{pmatrix} 4\cos\phi_1 + i2n_e^+\text{sen}\phi_1 & i2n_e^-\text{sen}\phi_1 \\ i2n_e^-\text{sen}\phi_1 & 4\cos\phi_1 - i2n_e^+\text{sen}\phi_1 \end{pmatrix}$$

where we defined

$$n_e^+ = \left(n_e + \frac{1}{n_e}\right), \qquad n_e^- = \left(n_e - \frac{1}{n_e}\right) \tag{15}$$

resulting in the following total transfer matrix

$$M = \mathcal{P}\begin{pmatrix} e^{i\phi_L} & 0 \\ 0 & e^{-i\phi_L} \end{pmatrix}\mathcal{P}\begin{pmatrix} e^{i\phi_R} & 0 \\ 0 & e^{-i\phi_R} \end{pmatrix}\mathcal{P}. \tag{16}$$

We next observe that $\phi_R = p\kappa a$ and $\phi_L = (1-p)\kappa a$, where $a = d_L + d_R$. Therefore, M depends upon p and $\boldsymbol{k}$ through κ and $k_{1,\perp}$, so in what follows we explicitly write $M \equiv M(\boldsymbol{k}, p)$. The transmittance is given by

$$T(\boldsymbol{k}, p) = \frac{1}{|M_{11}(\boldsymbol{k}, p)|^2}, \tag{17}$$

and for this particular case, the matrix element M_{11} is given by

$$M_{11}(\boldsymbol{k}, p) = \mathcal{P}_{11}^3 e^{i\kappa a} + \mathcal{P}_{12}^2\mathcal{P}_{22}e^{-i\kappa a} + 2\mathcal{P}_{11}\mathcal{P}_{12}^2\cos(1-2p)\kappa a, \tag{18}$$

where $\mathcal{P}_{ij}$ are the elements of matrix $\mathcal{P}$. Then,

$$T(\boldsymbol{k}, p) = \left|\mathcal{P}_{11}^3\right|^{-2}|e^{i\kappa a} + A(\boldsymbol{k})e^{-i\kappa a} + 2B(\boldsymbol{k})\cos[(1-2p)\kappa a]|^{-2} \tag{19}$$

with

$$A(\boldsymbol{k}) \equiv |A(\boldsymbol{k})|e^{i\phi_A} = (\mathcal{P}_{22}/\mathcal{P}_{11})B(\boldsymbol{k}), \tag{20}$$

$$B(\boldsymbol{k}) \equiv |B(\boldsymbol{k})|e^{i\phi_B} = (\mathcal{P}_{12}/\mathcal{P}_{11})^2. \tag{21}$$

Explicitly, $A(\boldsymbol{k})$ and $B(\boldsymbol{k})$ can be written as

$$A(\boldsymbol{k}) = -\frac{1-ib_-(k_{1,\perp})}{1+ib_+(k_{1,\perp})}B(\boldsymbol{k}), \tag{22}$$

$$B(\boldsymbol{k}) = -\left(\frac{b_-(k_{1,\perp})}{1+ib_+(k_{1,\perp})}\right)^2 \tag{23}$$

with

$$b_\pm(k_{1,\perp}) = \frac{n_e^\pm}{2}\tan\phi_1 = \frac{n_e^\pm}{2}\tan(k_{1,\perp}d_1). \tag{24}$$

Finally, we arrive at the following expression for the s-polarized transmittance valid for any kind of media:

$$T(\boldsymbol{k}, p) = \left|\mathcal{P}_{11}^3\right|^{-2}(1 + |A(\boldsymbol{k})|^2 + 4|B(\boldsymbol{k})|^2\cos^2[(1-2p)\kappa a] + 2|A(\boldsymbol{k})|\cos(2\kappa a - \phi_A) + 4|B(\boldsymbol{k})|\cos(\kappa a - \phi_B)\cos[(1-2p)\kappa a] + 4|A(\boldsymbol{k})||B(\boldsymbol{k})|\cos[(1-2p)\kappa a]\cos[\kappa a + \phi_B - \phi_A])^{-1}. \tag{25}$$

In Fig. 2 we present the resulting s-polarized transmittance as a function of the dimensionless variable $k_\parallel a$ and p for a cavity length $a = 6\lambda$. Notice that here we plot the transmittance as a function of the variable $k_\parallel$ as usually done in experiments. Direct numerical calculation using Eq. (11) shows perfect agreement with Fig. 2. The most remarkable feature is the presence of two families of high-transmittance curves. To understand such pattern we observe from Eq. (16) that inside the left or right cavity the maximal transmittance is obtained whenever $\phi_L = \pi m_L$ or $\phi_R = \pi m_R$ with m_L and m_R integers. Using the actual values of ϕ_L and ϕ_R we obtain that $p\kappa a = \pi m_R$ and $(1-p)\kappa a = \pi m_L$. This results in two expressions akin to the Bragg conditions,

$$2pa\cos\theta_0 = m_R\lambda, \tag{26}$$

$$2(1-p)a\cos\theta_0 = m_L\lambda. \tag{27}$$

On the other hand, within each cavity, the minimal transmission is obtained for $\phi_L = \pi m_L + \pi/2$ or $\phi_R = \pi m_R + \pi/2$.

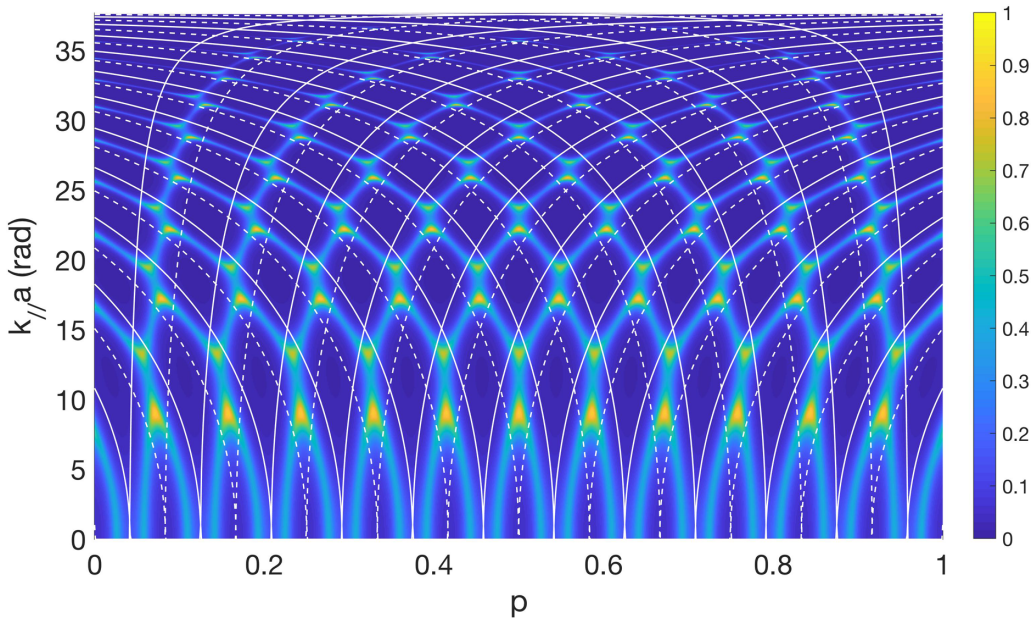

FIG. 2. s-polarized transmittance as a function of p and $k_\parallel a$ for $\lambda = 535$ nm, with $a = 6\lambda$. To the right we indicate the color code associated with the transmittance. The solid curves are obtained from the conditions $\phi_L = \pi m_L$ and $\phi_R = \pi m_R$, while the dotted curves correspond to the conditions $\phi_R = \pi m_R + (\pi/2)$ and $\phi_L = \pi m_L + (\pi/2)$. m_L and m_R are integers from 0 to 11.

Thus, the maximal scattering is given by two families of curves, which results in another set of conditions,

$$2pa\cos\theta_0 = (m_R + 1/2)\lambda, \tag{28}$$

$$2(1-p)a\cos\theta_0 = (m_L + 1/2)\lambda. \tag{29}$$

Figure 2 presents, using continuous and dashed white curves, the families of curves defined by Eqs. (26)–(29). Clearly, these families reveal the basic shape of the pattern. Observe how the pattern can be labeled with two indices (m_L, m_R). This is reminiscent of a diffraction produced by a 2D lattice which requires two Miller indices to label Bragg reflections. Such observation is the first hint to relate the coupled cavity to a synthetic triangular lattice via the pattern shown in Fig. 2. This analogy will be discussed in detail in the following sections.

Close to the intersections of all diffracted orders, the high-transmittance curves exhibit the typical splitting associated with the strong coupling between the modes of the individual cavities. This is induced by the condition on the semitransparency of the mirrors and maximized by the chosen central mirror thickness. To better understand the mode coupling and the origin of the transmittance pattern, in Fig. 3 we calculate the modes dispersion of the coupled cavity for $a = 6\lambda$ and $p = 0.5$. Here, the high-transmittance pairs of parabolas correspond to the splittings observed in Fig. 2 for $p = 0.5$ and for the energy of $\hbar 2\pi c/\lambda$. The mode dispersion of the coupled cavity qualitatively resembles that of the cavity modes sustained by each individual cavity, with an energy shift and a modulation in transmittance intensity provided by the second cavity. To understand this, we observe that for an individual cavity filled with air, the photon energy is given by [39]

$$E(k_\parallel) \approx \hbar c\sqrt{\left(\frac{m\pi}{a}\right)^2 + k_\parallel^2}, \tag{30}$$

where m is an integer. This relationship produces a set of displaced parabolas for different m. Once a second cavity is added, an energy shift and modulation in transmittance occur simultaneously to all parabolas and for each value of p. The plot of the transmittance pattern $T(\boldsymbol{k}, p)$ facilitates the analogy to a 2D lattice which would otherwise be very difficult to spot by only looking at the dispersion of the optical modes for different p.

In electronic systems, diffraction is associated with singularities in the density of states (DOS), known as Van Hove singularities. In our case we need to adapt the idea of a DOS and translate it into a distribution of transmittance, $\rho(T)$.

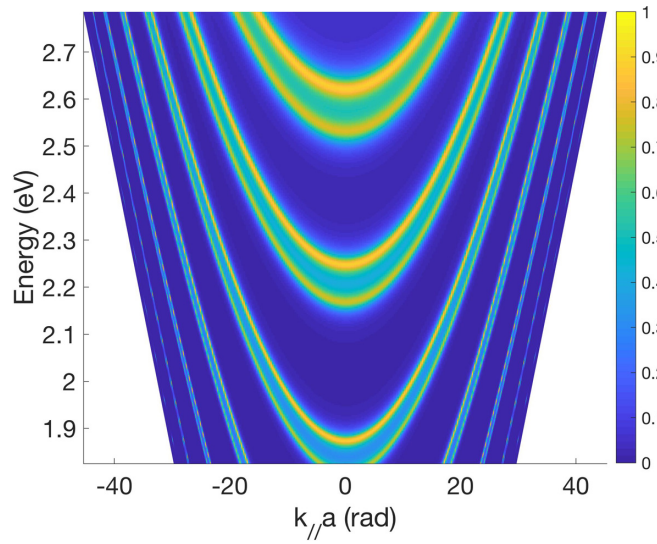

FIG. 3. s-polarized transmittance as a function of photon energy and $k_\parallel$ for $a = 6\lambda$ and $p = 0.5$. To the right we indicate the color code associated with the transmittance.

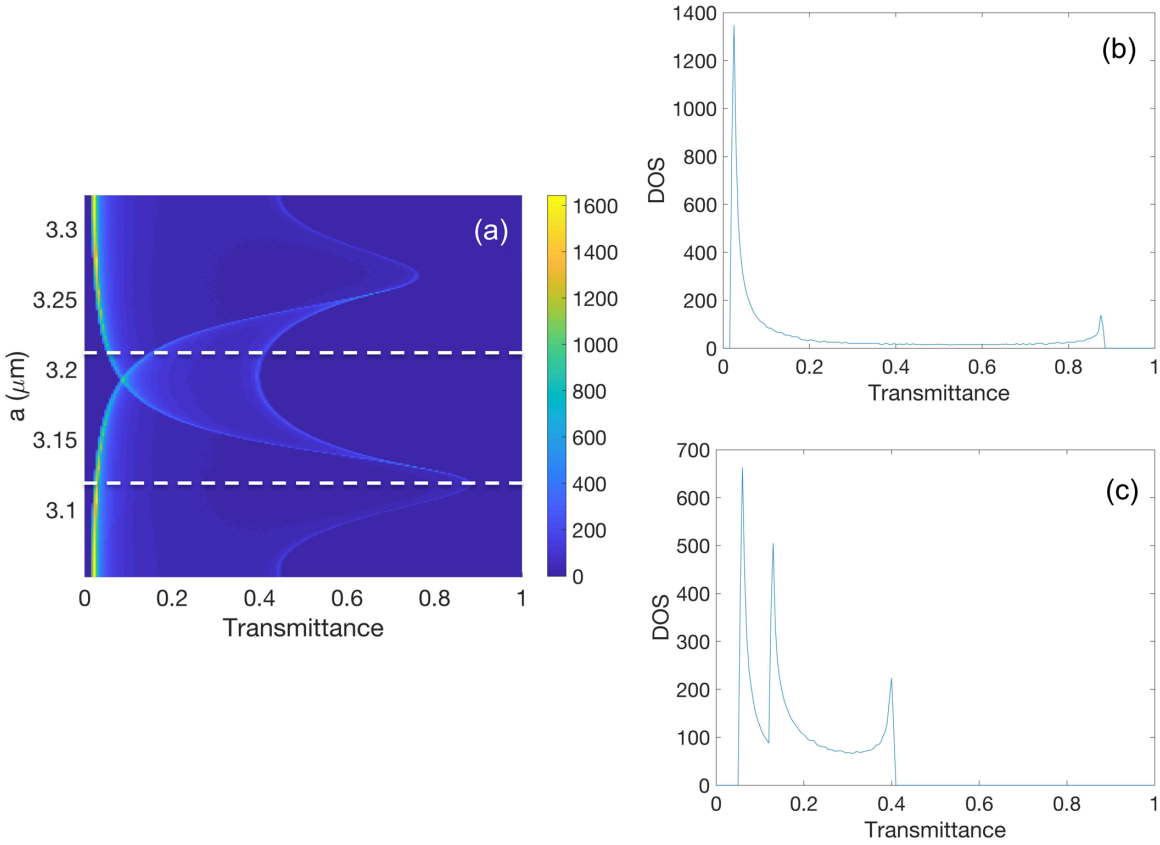

FIG. 4. (a) Transmittance distribution, $\rho_{\kappa a}(T)$, as a function of a and transmittance value calculated for $\theta_{\text{inc}} = 0$ and for $\lambda = 535$ nm. (b) and (c) are cuts of $\rho_{\kappa a}(T)$ corresponding to the dashed lines in (a). The peaks are equivalent to Van Hove singularities.

Considering all the κa as possible states of the system for a given cavity with fixed p and a,

$$\rho_p(T) = \int_0^\infty \delta(|M_{11}(\boldsymbol{k}, p)|^2 - T) dk_\parallel. \tag{31}$$

Similarly, if we fix the frequency ω and the angle of incidence is such a way that $\boldsymbol{k}$ is fixed, we obtain the transmittance distribution over all possible coupled cavities for a given total cavity length, a,

$$\rho_{ka}(T) = \int_0^\infty \delta(|M_{11}(\boldsymbol{k}, p)|^2 - T) dp. \tag{32}$$

Finally, we can obtain the total density for all possible cavities,

$$\rho(T) = \int_0^1 \int_0^\infty \delta(|M_{11}(\boldsymbol{k}, p)|^2 - T) dp\, dk_\parallel. \tag{33}$$

Figure 4(a) presents $\rho_{\kappa a}(T)$ as a function of a and transmittance calculated at normal incidence. The sharp features correspond to specific transmittance values highly encountered for each total cavity length. The number of peaks varies between two and three depending on a and their values span almost all transmittance axes. The pattern observed in Fig. 4(a) repeats itself for larger and smaller values of a providing a compact and complementary way to describe the pattern shown in Fig. 2 which was obtained for a fixed a. This periodicity is strictly related to the Bragg's law [see Eqs. (26)–(29)]. In the next section we will see how the transmittance pattern is associated to a synthetic modulated 2D lattice.

III. SYNTHETIC DIMENSION IN A COUPLED CAVITY AND ANALOGY WITH A 2D ELECTRONIC SYSTEM

In this section we discuss how to perform an analogy with 2D electronic systems. To simplify the discussion, we assume that the system absorbs very little energy as we deal with very narrow mirrors. This provides a way to compare with a usual conservative and stationary quantum mechanical system. Such assumption can be relaxed at the price of having a non-Hermitian Hamiltonian. Under the assumption of small energy absorption we have that $A(\boldsymbol{k}) \approx e^{ib_+(k_{1\perp})} B(\boldsymbol{k})$ from where $|A(\boldsymbol{k})| = |B(\boldsymbol{k})|$. Also, $T(\boldsymbol{k}, p)$ can be considered as a function of two independent variables, κa and p. To highlight such fact we make the following coordinate transformation:

$$k_x = \kappa, \tag{34}$$

$$k_y = (1 - 2p)\kappa. \tag{35}$$

Observe that this transformation induces a deformation of the domain, i.e., the square grid produced by lines of the type $k_x = C$ or $k_y = C$ with C a constant, is mapped into hyperbolas. After this coordinate transformation, Eq. (25) is written as

$$\begin{aligned} T(k_x, k_y) = \left|\mathcal{P}_{11}^3\right|^{-2} (1 + 2|A(k_x)|[&\cos(2k_x a - \phi_A) \\ &+ 2\cos(k_x a - \phi_B)\cos(k_y a)] \\ &+ |A(k_x)|^2[1 + 4\cos^2(k_y a) \\ &+ 4\cos(k_y a)\cos(k_x a + \theta_B - \theta_A)])^{-1}, \end{aligned} \tag{36}$$

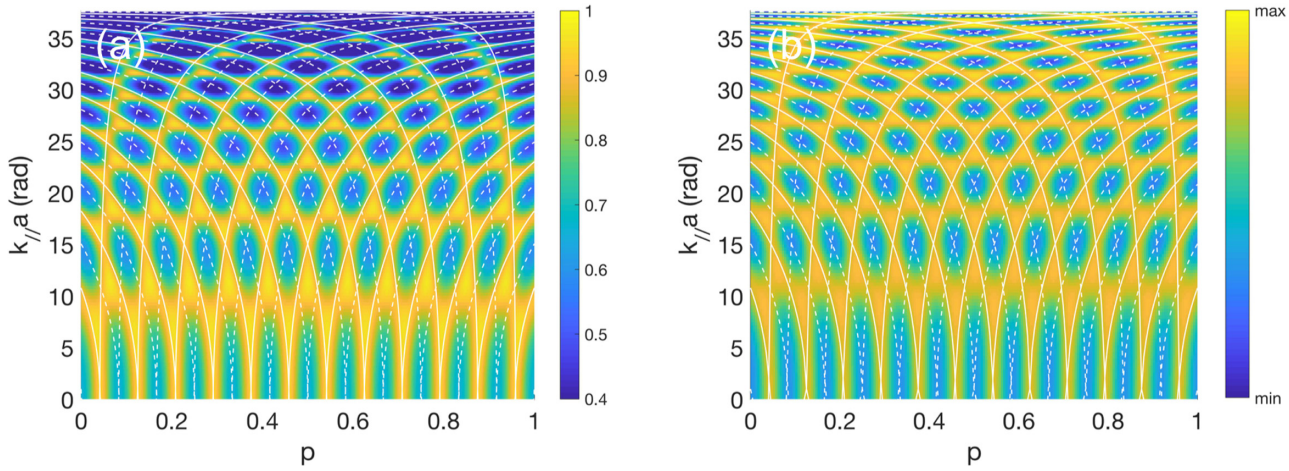

FIG. 5. (a) Very thin mirror limit ($d_1 = 3$ nm) exact s-polarized transmittance as a function of $k_\parallel a$ and p, calculated for $\lambda = 535$ nm using Eq. (25). (b) s-polarized transmittance calculated using the approximation given by Eq. (38), and the coordinate transformation obtained by inverting Eqs. (34) and (35) for the same mirror thickness as in (a). Dotted and continuous curves are as in Fig. 2. By comparing panel (a) with (b) we see that the approximated transmittance matches well the exact calculation up to $k_\parallel a \approx 20$ as this requires $A(k_x)$ to be constant. Thus the analogy with a triangular lattice is restricted to a range of incidence angles and thin mirrors. Also notice the difference between panel (a) and Fig. 2 due to the different mirror thickness. The thickness change broadens the transmittance features and slightly shifts them, making the overlap between the diffraction pattern and the high-transmittance regions slightly different. It involves not only a different amount of optical absorption but also an overall phase change in the waves propagating through the system.

where $A(\boldsymbol{k}) = A(k_x)$ and $B(\boldsymbol{k}) = B(k_x)$. In the limit of very narrow mirrors, i.e., $\phi_1 \ll 1$, from Eqs. (20) and (21) we see that $A(k_x) \ll 1$. Therefore, Eq. (36) can be written as

$$T(k_x, k_y) \approx \left|\mathcal{P}_{11}^3\right|^{-2}\{1 - 2|A(k_x)|[\cos(2k_x a - \phi_A) + 2\cos(k_x a - \phi_B)\cos(k_y a)]\}. \tag{37}$$

In the same limit, due to the lack of absorption in the mirrors, we have that $\phi_A = 0$, $\phi_B = 0$, and by considering $\mathcal{P}_{11} \approx 1$ we obtain

$$T(k_x, k_y) \approx 1 - 2|A(k_x)|[\cos(2k_x a) + 2\cos(k_x a)\cos(k_y a)]. \tag{38}$$

Figure 5(a) displays the s-polarized transmittance, calculated using Eq. (25), as a function of $k_\parallel a$ and p for the case of very thin silver mirrors, i.e., $d_1 = 3$ nm. Even though the broadening induced by the nonoptimal coupling condition between the left and right cavities masks the mode splitting, by comparing Figs. 5(a) and 2 we notice that the transmittance pattern is the same. This calculation is compared with the one based on Eq. (38) [Fig. 5(b)] which is only valid in the case of thin, nonabsorbing mirrors. Notice that in order to allow the direct comparison with Fig. 5(a), in Fig. 5(b) we plot T as a function of $k_\parallel a$ and p instead of k_x and k_y. This is done by inverting the coordinate transformation, Eqs. (34) and (35). We obtain an excellent qualitative agreement between the calculations shown in (a) and (b). Both follow the diffracted orders plotted in Fig. 2 and displayed with white continuous and dotted curves. The only difference appreciated in (b) with respect to (a) is that at the crossing points of the diffracted orders the transmittance increases as $k_\parallel a$ grows instead of decreasing. This is simply due to the approximations made to obtain Eq. (38). We stress that, due to the approximations and simplifications made in the algebraic derivation, the transmittance calculated with Eq. (38) and shown in Fig. 5(b) is not normalized. For this reason we do not report numeric values in the color scale, but rather we focus on its qualitative pattern.

As is very well known, optical layered systems described by transfer matrices are suitable to be interpreted as a chain of atoms approximated by a tight-binding Hamiltonian [40]. Under this analogy, the left and right media cavities can be associated to a certain type of atom while the mirror media to another type. Then, if we consider p as a variable, the resulting system can be considered as a 2D system. However, the simplest way to arrive at such analogy is to compare Eq. (38) with the energy dispersion resulting from a 2D electronic system, instead of building the whole transfer matrix analogy.

Following this approach, let us now draw explicitly the analogy with an electronic 2D system by comparing Eq. (38) with the energy dispersion that results from an electron in a uniaxial strained triangular lattice using a tight-binding Hamiltonian [41–43]. To do so, first consider the jth atom position on a triangular lattice with a uniform strain along the y direction,

$$\boldsymbol{r}_j = j_1\boldsymbol{b}_1 + j_2\boldsymbol{b}_2. \tag{39}$$

Here $\boldsymbol{b}_1 = b_1(1, 0)$ and $\boldsymbol{b}_2 = (b_1\cos(2\pi/3), b_2\sin(2\pi/3))$ are the Bravais lattice vectors and j_1, j_2 integers. b_1 is the separation between atoms in the x direction and $b_2 = (1 + \epsilon)b_1$, where ϵ is the strain in the y direction, assumed here to be small ($\epsilon \ll 1$). For the case of atoms with only one valence orbital, the corresponding tight-binding Hamiltonian is

$$H = \epsilon_0|j\rangle\langle j| + t_0\sum_{(l,j)}|l\rangle\langle j|, \tag{40}$$

where $|j\rangle$ is a Wannier orbital localized at site j, ϵ_0 is the self-energy, and t_0 is the hopping parameter between first-neighbor sites l and j. Using Bloch's theorem in the Schrödinger equation $H|\Psi\rangle = E|\Psi\rangle$, where E is the energy and Ψ the wave

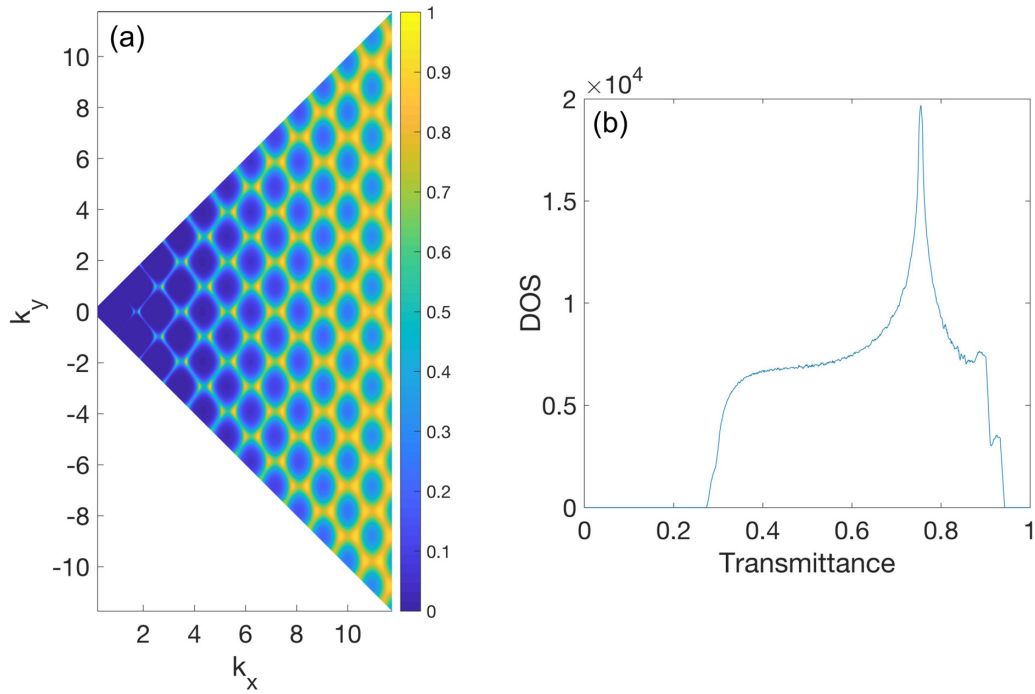

FIG. 6. (a) s-polarized transmittance calculated for a mirror thickness $d_1 = 5$ nm and transformed according to Eqs. (34) and (35). (b) Transmittance distribution as a function of the transmittance value calculated in the interval $k_x = [9.3, 9.8]$. The geometrical pattern of the transmittance and its single-peak distribution show explicitly the analogy between the transmittance pattern of the 1D coupled optical cavity and the energy of a modulated 2D triangular lattice. Two extra peaks for high transmittance are seen when compared with the electronic case; these are due to the finite mirror thickness and can be removed either by reducing its thickness or by processing the optical data taking into account a mirror correction factor $A(k_x)$.

function, we have that

$$E|j\rangle = \epsilon_0|j\rangle + t_0 \sum_{n=1}^{6} e^{i\boldsymbol{k}\cdot\boldsymbol{\delta}_n}|j\rangle, \tag{41}$$

where $\boldsymbol{\delta}_n$ is the set of vectors that point from a site to its first nearest neighbors, i.e., $\delta_{1,4} = \pm b_1(1, 0)$, $\delta_{2,5} = \pm(-b_1/2, \sqrt{3}b_2/2)$, $\delta_{3,6} = \pm(b_1/2, \sqrt{3}b_2/2)$. By using these vectors in Eq. (41) we arrive at

$$E(\boldsymbol{k}) = (\epsilon_0 - 3t_0) - 2t_0\left[\cos(k_x b_1) + 2\cos\left(\frac{k_x b_1}{2}\right)\right.$$
$$\left.\times\ \cos\left(\frac{\sqrt{3}k_y b_2}{2}\right)\right]. \tag{42}$$

Compare this result with Eq. (38). If we set $b_1 = a/2$ and $b_2 = 2a/\sqrt{3}$, the arguments and phases of the cosines coincide. Moreover, as in this regime $|A(\boldsymbol{k})| \approx |B(\boldsymbol{k})|$, it is tempting to identify,

$$t_0 \to A(k_x), \quad \epsilon_0 = 1 + 3t_0. \tag{43}$$

This mathematical correspondence explains why the transmittance pattern of the 1D coupled cavity sketched in Fig. 1 resembles the energy dispersion of a 2D strained triangular lattice. The mode coupling induced by the moving mirror generates an extra synthetic dimension allowing the 1D cavity to simulate a tight-binding Hamiltonian built on a 2D lattice. Similarly, the peaks observed in the transmittance distribution in Figs. 4(b) and 4(c) are akin to the Van Hove singularities typically found in atomic crystals. We stress that such lattice symmetry is interesting in the context of 2D materials [44–47]. Furthermore, applying strain to control the electronic properties of such materials gave birth to a new field of research called straintronics [43,48]. Summarizing, (i) the moving mirror, parametrized by p, together with the semi-transparency of the left and right mirrors, generate a synthetic 2D lattice; (ii) the crossing of the two families of diffracted orders dictates the triangular lattice symmetry; and (iii) the thickness of the central mirror determines the visibility of the mode spitting at the crossing points.

The identification proposed in Eq. (43) is not entirely exact as t_0 is a constant and $A(k_x)$ depends upon k_x. To overcome this problem, observe that Eq. (42) can be used with a given fixed t_0 only for a certain range of k as $A(k_x)$ varies much slower than the cosine factors, implying that the whole spectrum is obtained by scaling Eq. (42) as k is changed. The coordinate transformation from (k_x, k_y) to $(k_\parallel, p)$ produces a pattern like the one seen in Fig. 2, i.e., a hyperbolic deformed triangular structure that repeats itself but scales down as $k_\parallel a \to \infty$. Notice that such scaling is also modulated by the term $|\mathcal{P}_{11}^3|^{-2}$ which provides an intensity modulation, but is not responsible for the "reduction" of the hexagons size and deformation as $k_\parallel a \to \infty$. A complementary way to understand the analogy is to consider a space-dependent modulation of the tight-binding parameter of the strained triangular lattice [49].

To explicitly show the analogy of the 1D coupled cavity with the moving mirror and the 2D triangular atomic lattice we apply the transformation given in Eqs. (34) and (35) to the transmittance calculated with Eq. (25). Figure 6(a) displays the resulting s-polarized transmittance as a function of the

transformed coordinates (k_x, k_y) for a cavity length $a = 6\lambda$ and for thin mirrors, $d_1 = 5$ nm. The transformed transmittance pattern is symmetric with respect to k_y as expected by the mirror symmetry of $T(k_\parallel a, p)$ with respect to p. We see that the regular triangular pattern is recovered while the modulation introduced by the term $A(k_x)$ is maintained. For this reason, and as already noticed above, the analogy with the tight-binding model only holds for a certain range of k_x. By calculating the transmittance distribution integrating in the range $k_x = [9.3, 9.8]$ we recover the typical single-peak density of states of a triangular lattice. This is shown in Fig. 6(b) which further helps in clarifying the relation between the 1D optical cavity and the 2D modulated lattice. By making the term $A(k_x)$ flatter the range of integration can be extended while maintaining the single-peak transmittance distribution. This condition can be met by designing a mirror with a less pronounced angle-dependent reflectance.

The analogy with an electronic system allows one to extract some other physical quantities from the optical system. Among these, the most important is the group velocity $\boldsymbol{v}_g(\boldsymbol{k})$ which can be used, for example, to find the electronic conductivity through the Boltzmann formula. If a stationary electric field $\boldsymbol{E}$ is applied to an electronic system, the Boltzmann equation for the current density at zero temperature and Fermi energy E_F is given by [50]

$$\boldsymbol{J} = \frac{e^2}{(2\pi)^2} \int d^2\boldsymbol{k}[\boldsymbol{E} \cdot \boldsymbol{v}_g(\boldsymbol{k})]\tau(\boldsymbol{k})\boldsymbol{v}_g(\boldsymbol{k})\delta[E(\boldsymbol{k}) - E_F], \quad (44)$$

where $\tau(\boldsymbol{k})$ is the relaxation time, usually taken as a constant τ fitted from experiment. It can also be calculated using an integral equation [51]. For an electric field in the x direction $\boldsymbol{E} = (E_x,\ 0)$, the conductivities are given by $\sigma_{xx} = J_x/E_x$ and $\sigma_{yx} = J_y/E_x$. Therefore, the main ingredients to calculate the conductivity are the density of states near E_F, which appears through the integral and the delta function in Eq. (44), and the group velocity, given by

$$\boldsymbol{v}_g(k) = (1/\hbar)\nabla_{\boldsymbol{k}} E(\boldsymbol{k}) = (1/\hbar)\nabla_{\boldsymbol{k}} T(\boldsymbol{k}), \quad (45)$$

where the last step follows from the optical analogy, i.e., Eq. (38). Therefore, the gradient of the transmittance pattern provides $\boldsymbol{v}_g(\boldsymbol{k})$. Using Eq. (38) we can obtain its explicit form,

$$\boldsymbol{v}_g(\boldsymbol{k}) \approx 4|A(k_x)|(\sin(2k_x a) + \sin(k_x a) \times \cos(k_y a), \cos(k_x a)\sin(k_y a)), \quad (46)$$

where we neglected the term proportional to $\nabla_{\boldsymbol{k}}|A(k_x)|$ as it is very small in the integration region. The conductivities can be obtained from the optical analogy just by considering the Jacobian of the transformation given by Eqs. (34) and (35) and that the Fermi energy, E_F, is the photon energy corresponding to the wavelength of the wave incident on the cavity,

$$\sigma_{\beta x} \approx \frac{2e^2\tau}{(2\pi)^2} \iint d\kappa\, dp\, v_g^x(\boldsymbol{k}) v_g^\beta(\boldsymbol{k})\delta[T(\boldsymbol{k}) - E_F], \quad (47)$$

where v_g^β with $\beta = x, y$ are the components of $\boldsymbol{v}_g$ and it is understood that $\boldsymbol{k}$ is evaluated through Eqs. (34) and (35).

Finally, it is interesting to observe that Van Hove singularities arise whenever Bragg conditions hold as diffraction implies standing waves and thus $\boldsymbol{v}_g(k) = 0$. Moreover, Van Hove singularities encode topological information about the Hamiltonian in the bulk system [50,52,53] and thus some properties of topological boundary states can be inferred by perturbing near such singularities [54]. The procedure can be applied to the quantum Hall effect [53,54] or to strained graphene nanoribbons [42]. Its use in optical analogies in the present context will require either studying small variations of p around such singularities [42] or a periodic adiabatic time driving [55], achieved, for example, by moving the central mirror.

IV. TRULY SYNTHETIC DIMENSION: IRRATIONAL CAVITY LENGTH RATIOS

Up to this point, we have considered generating a synthetic dimension by a moving mirror. This connection with synthetic dimensions seems a bit stretched because we have two continuous parameters, p and k, which are connected then with two dimensions k_x and k_y in the electron system. In other words, we considered p as a variable that can be tuned freely. There are two ways to experimentally study such a system: fabricating many different devices or wedging the middle mirror allowing for a continuous variation of p in a single device. The former one is unpractical for real world application, while the latter one involves a large single device with nonparallel interfaces that may disturb the diffraction coupling mechanism. In spite of the practical details, none of these alternatives contain a truly synthetic dimension. Below we will show that for a fixed p, provided that p is chosen to be an irrational number, the system contains a synthetic dimension. To do so, notice that any number x can be decomposed as $x = \lfloor x \rfloor + \{x\}$ where $\lfloor x \rfloor$ is the bigger integer lower than x (floor function) and $\{x\}$ its fractional part (sawtooth function). Using such decomposition, the cosine terms containing p in Eq. (25) can be written

$$\cos[(1-2p)\kappa a] = \cos\left(2\pi\left\{\frac{(1-2p)\kappa a}{2\pi}\right\}\right). \quad (48)$$

For any irrational p, the number $1 - 2p$ is also an irrational. In such case, the function $\{(1-2p)\kappa a\}$ behaves as a pseudo-random number generator [5] and thus is almost independent on κa. Therefore, we can replace the factor $\{(1-2p)\kappa a/2\pi\}$ by

$$2\pi\left\{\frac{(1-2p)\kappa a}{2\pi}\right\} \equiv k_y a, \quad (49)$$

where we defined a new wave vector k_y. Now k_x and k_y are almost independent variables for a fixed p. As explained before, this is a consequence of the decoupling of wave phases at irrational values of p. A more intuitive way to understand the phenomena is to think on the fact that resonant modes in one cavity are never resonant in the other as this will require a rational ratio between wave lengths. Therefore, we achieved a way to reach the 2D system for a fixed parameter p. Notice that in our proposed system the synthetic dimension is continuous as we can obtain $E(\boldsymbol{k})$ for any arbitrary vector $\boldsymbol{k}$ in 2D, as the components k_x and k_y are arbitrary. This is different from other optical systems in which discreteness is crucial in the sense that in a continuous three-dimensional space one can create a four-dimensional system but the latter must be discrete and not continuous [56]. Here, the continuous

sampling of one variable (k_x) leads to an independent, almost random, sampling of the other variable (k_y) for irrational fixed p. This is simple to understand if we think that points in a cartesian plane of the form (x, y) with $y = f(x) = \{xp\}$, for irrational p, will fill in a uniform and dense way a unitary square when x is continuously varied from zero to one [5].

Of course, in practice there is not infinite precision for fabricating the system and thus reach a truly irrational p. In spite of this, there are certain p values which are better than others. In particular, the approximants of the inverse golden mean cavity with $p = (\sqrt{5} - 1)/2$, given by the ratio of two successive Fibonacci numbers, is the best experimental choice. This is because the continued fraction expansion of the golden mean is the slowest convergent one among all p, making it the "most irrational" number. Using quasi-irrational cavity length ratios helps in bringing the concept of synthetic dimensions in 1D optical cavities closer to experimental possibilities, making the device compact and avoiding working with a set of different 1D cavities.

V. CONCLUSIONS

In this work we proposed a geometric method to generate synthetic dimensions. In particular we considered two optical cavities separated by a semitransparent moving mirror. We calculated the transmittance as a function of two variables: the in-plane momentum and the position of the coupling mirror. We proved that this transmittance pattern can be described by Bragg diffraction using two indices, indicating that the second variable acts as an effective momentum and adds a synthetic dimension to the system. We demonstrate the optical transmittance pattern corresponds to an isoenergetic plane of the dispersion of an electron in a 2D strained triangular lattice calculated with a tight-binding model. As a consequence, the transmittance distribution can be associated with the density of states of such lattice and, as such, it presents the equivalent of Van Hove singularities. This analogy makes the 1D optical cavity an efficient simulator for complex 2D Hamiltonians, bringing together two seemingly unrelated research fields.

Finally, we showed that the truly synthetic dimension in planar cavities appears by using the golden ratio between the two internal characteristic lengths. In this case, the reflected and transmitted electromagnetic waves have phases that behave as almost independent variables decoupling the modes of each cavity. Such decomposition for a fixed irrational cavity effectively nests two dimensions into one. Our study opens the door to use this simple principle to design and build synthetic dimensions in a systematic way. Compact devices made by coupled 1D optical cavities may be beneficial for bringing the concept of synthetic dimensions closer to real world applications.

Note added. Recently, we became aware of a work that studied topological boundary effects using synthetic frequency dimensions. The device is made of two ring cavities of different lengths that interact through an electro-optic modulator [57]. The advantage of our design is that it naturally includes such boundary as p is bounded between 0 and 1.

ACKNOWLEDGMENTS

This work was supported by Grants UNAM DGAPA PAPIIT No. IN102620 and No. IN104522 and CONACyT projects 1564464 and 1098652.

[1] L. Yuan, Q. Lin, M. Xiao, and S. Fan, Optica **5**, 1396 (2018).
[2] T. Ozawa and H. M. Price, Nat. Rev. Phys. **1**, 349 (2019).
[3] Q. Wang, M. Xiao, H. Liu, S. Zhu, and C. T. Chan, Phys. Rev. X **7**, 031032 (2017).
[4] O. Boada, A. Celi, J. I. Latorre, and M. Lewenstein, Phys. Rev. Lett. **108**, 133001 (2012).
[5] C. Janot, *Quasicrystals: A Primer*, Monographs on the Physics and Chemistry of Materials (Oxford University Press, Oxford, 2012).
[6] W. Steurer and S. Deloudi, *Crystallography of Quasicrystals* (Springer-Verlag, Berlin Heidelberg, 2009), Vol. 126, pp. 61–186.
[7] M. Baake and U. Grimm, *Aperiodic Order*, Encyclopedia of Mathematics and its Applications Vol. 2 (Cambridge University Press, Cambridge, UK, 2017).
[8] C. R. Dean, L. Wang, P. Maher, C. Forsythe, F. Ghahari, Y. Gao, J. Katoch, M. Ishigami, P. Moon, M. Koshino, T. Taniguchi, K. Watanabe, K. L. Shepard, J. Hone, and P. Kim, Nature (London) **497**, 598 (2013).
[9] A. Regensburger, C. Bersch, M.-A. Miri, G. Onishchukov, D. N. Christodoulides, and U. Peschel, Nature (London) **488**, 167 (2012).
[10] T. Ozawa, H. M. Price, N. Goldman, O. Zilberberg, and I. Carusotto, Phys. Rev. A **93**, 043827 (2016).
[11] D. Leykam and S. Flach, APL Photonics **3**, 070901 (2018).
[12] E. Lustig, S. Weimann, Y. Plotnik, Y. Lumer, M. A. Bandres, A. Szameit, and M. Segev, Nature (London) **567**, 356 (2019).
[13] Z. Yang, E. Lustig, G. Harari, Y. Plotnik, Y. Lumer, M. A. Bandres, and M. Segev, Phys. Rev. X **10**, 011059 (2020).
[14] C. Qin, F. Zhou, Y. Peng, D. Sounas, X. Zhu, B. Wang, J. Dong, X. Zhang, A. Alù, and P. Lu, Phys. Rev. Lett. **120**, 133901 (2018).
[15] B. A. Bell, K. Wang, A. S. Solntsev, D. N. Neshev, A. A. Sukhorukov, and B. J. Eggleton, Optica **4**, 1433 (2017).
[16] L. Yuan, A. Dutt, M. Qin, S. Fan, and X. Chen, Photonics Res. **8**, B8 (2020).
[17] M. Kremer, I. Petrides, E. Meyer, M. Heinrich, O. Zilberberg, and A. Szameit, Nat. Commun. **11**, 907 (2020).
[18] Y. E. Kraus and O. Zilberberg, Phys. Rev. Lett. **109**, 116404 (2012).
[19] Y. E. Kraus, Y. Lahini, Z. Ringel, M. Verbin, and O. Zilberberg, Phys. Rev. Lett. **109**, 106402 (2012).
[20] A. Gómez-León and G. Platero, Phys. Rev. Lett. **110**, 200403 (2013).
[21] P. Roman-Taboada and G. G. Naumis, Phys. Rev. B **95**, 115440 (2017).
[22] P. Roman-Taboada and G. G. Naumis, J. Phys. Commun. **1**, 055023 (2017).

[23] L. Yuan, Y. Shi, and S. Fan, Opt. Lett. **41**, 741 (2016).
[24] X.-W. Luo, X. Zhou, J.-S. Xu, C.-F. Li, G.-C. Guo, C. Zhang, and Z.-W. Zhou, Nat. Commun. **8**, 16097 (2017).
[25] C. Weisbuch, M. Nishioka, A. Ishikawa, and Y. Arakawa, Phys. Rev. Lett. **69**, 3314 (1992).
[26] F. Baboux, L. Ge, T. Jacqmin, M. Biondi, E. Galopin, A. Lemaître, L. Le Gratiet, I. Sagnes, S. Schmidt, H. E. Türeci, A. Amo, and J. Bloch, Phys. Rev. Lett. **116**, 066402 (2016).
[27] X. Liu, T. Galfsky, Z. Sun, F. Xia, E.-c. Lin, Y.-H. Lee, S. Kéna-Cohen, and V. M. Menon, Nat. Photonics **9**, 30 (2015).
[28] D. G. Lidzey, D. D. C. Bradley, M. S. Skolnick, T. Virgili, S. Walker, and D. M. Whittaker, Nature (London) **395**, 53 (1998).
[29] J. Kasprzak, M. Richard, S. Kundermann, A. Baas, P. Jeambrun, J. M. J. Keeling, F. M. Marchetti, M. H. Szymańska, R. André, J. L. Staehli, V. Savona, P. B. Littlewood, B. Deveaud, and L. S. Dang, Nature (London) **443**, 409 (2006).
[30] G. Lerario, A. Fieramosca, F. Barachati, D. Ballarini, K. S. Daskalakis, L. Dominici, M. De Giorgi, S. A. Maier, G. Gigli, S. Kéna-Cohen, and D. Sanvitto, Nat. Phys. **13**, 837 (2017).
[31] A. Amo, S. Pigeon, D. Sanvitto, V. G. Sala, R. Hivet, I. Carusotto, F. Pisanello, G. Leménager, R. Houdré, E. Giacobino, C. Ciuti, and A. Bramati, Science **332**, 1167 (2011).
[32] P. C. Holz, S. Auchter, G. Stocker, M. Valentini, K. Lakhmanskiy, C. Rössler, P. Stampfer, S. Sgouridis, E. Aschauer, Y. Colombe, and R. Blatt, Adv. Quamtum Technol. **3**, 2000031 (2020).
[33] S. Kéna-Cohen and S. R. Forrest, Nat. Photonics **4**, 371 (2010).
[34] T. Yagafarov, D. Sannikov, A. Zasedatelev, K. Georgiou, A. Baranikov, O. Kyriienko, I. Shelykh, L. Gai, Z. Shen, D. Lidzey, and P. Lagoudakis, Commun. Phys. **3**, 18 (2020).
[35] A. V. Zasedatelev, A. V. Baranikov, D. Sannikov, D. Urbonas, F. Scafirimuto, V. Y. Shishkov, E. S. Andrianov, Y. E. Lozovik, U. Scherf, T. Stöferle, R. F. Mahrt, and P. G. Lagoudakis, Nature (London) **597**, 493 (2021).
[36] T. W. Ebbesen, Acc. Chem. Res. **49**, 2403 (2016).
[37] J. Yuen-Zhou and V. M. Menon, Proc. Natl. Acad. Sci. USA **116**, 5214 (2019).
[38] P. Yeh, *Optical Waves in Layered Media*, Wiley Series in Pure and Applied Optics (Wiley, New York, 2005).
[39] V. M. Agranovich, M. Litinskaia, and D. G. Lidzey, Phys. Rev. B **67**, 085311 (2003).
[40] M. Kohmoto, B. Sutherland, and K. Iguchi, Phys. Rev. Lett. **58**, 2436 (1987).
[41] M. Oliva-Leyva and G. G. Naumis, Phys. Rev. B **88**, 085430 (2013).
[42] G. G. Naumis and P. Roman-Taboada, Phys. Rev. B **89**, 241404(R) (2014).
[43] G. G. Naumis, S. Barraza-Lopez, M. Oliva-Leyva, and H. Terrones, Rep. Prog. Phys. **80**, 096501 (2017).
[44] X. Duan, Z. Liu, B. M. Hanrahan, W. Zhu, and S. Liu, Phys. Rev. Materials **4**, 124003 (2020).
[45] X.-G. Zheng, I. Yamauchi, S. Kitajima, M. Fujihala, M. Maki, S. Lee, M. Hagihala, S. Torii, T. Kamiyama, and T. Kawae, Phys. Rev. Materials **2**, 104401 (2018).
[46] A. C. Dias, F. Qu, D. L. Azevedo, and J. Fu, Phys. Rev. B **98**, 075202 (2018).
[47] M. Bauernfeind, J. Erhardt, P. Eck, P. K. Thakur, J. Gabel, T.-L. Lee, J. Schäfer, S. Moser, D. Di Sante, R. Claessen, and G. Sangiovanni, Nat. Commun. **12**, 5396 (2021).
[48] F. Miao, S.-J. Liang, and B. Cheng, npj Quantum Mater. **6**, 59 (2021).
[49] G. García Naumis, Rev. Mex. Fís. **67**, 050102 (2021).
[50] W. Jones and N. March, *Theoretical Solid State Physics*, Dover Books on Physics and Chemistry Vol. 1 (Wiley-Interscience, New York, 1973).
[51] R. S. Sorbello, J. Phys. F **4**, 503 (1974).
[52] J. C. Phillips, Phys. Rev. **104**, 1263 (1956).
[53] G. Naumis, Phys. Rev. B **100**, 165101 (2019).
[54] G. G. Naumis, Phys. Lett. A **380**, 1772 (2016).
[55] V. G. Ibarra-Sierra, J. C. Sandoval-Santana, A. Kunold, S. A. Herrera, and G. G. Naumis, J. Phys.: Mater. **5**, 014002 (2022).
[56] D. Jukić and H. Buljan, Phys. Rev. A **87**, 013814 (2013).
[57] A. Dutt, L. Yuan, K. Y. Yang, K. Wang, S. Buddhiraju, J. Vučković, and S. Fan, Nat. Commun. **13**, 3377 (2022).